Naftali (Tuli) Herscovici
AnTeg
52 Agnes Drive
Framingham, MA 01901 USA
+1 (508) 788-5152
+1 (508) 788-6226 (Fax)
tuli@ieee.org (e-mail)

Christos Christodoulou
Department of Electrical and
Computer Engineering
University of New Mexico
Albuquerque, NM 87131-1356 USA
+1 (505) 277-6580
+1 (505) 277-1439 (Fax)
christos@eece.unm.edu (e-mail)

Smart-Antenna System for Mobile Communication Networks Part 2: Beamforming and Network Throughput

Salvatore Bellofiore, Jeffrey Foutz, Constantine A. Balanis, and Andreas S. Spanias

Department of Electrical Engineering, Telecommunications Research Center
Arizona State University, Tempe, AZ 85287-7206 USA
Tel: +1 (480) 965-3909; E-mail: balanis@asu.edu

Abstract

Part 1 of this paper provided an overview of smart-antenna systems, and presented a planar array as a design example. In addition, Part I discussed the potential of smart antennas with regard to providing increased capacity in wireless communication networks. Part 2 represents a continuation of the previous paper, and introduces the signal-processing aspects of the antenna array. In particular, Part 2 describes the utility of direction-of-arrival algorithms in array-antenna systems, and gives an overview of the signal-processing algorithms that are used to adapt the antenna radiation pattern. The adaptive-algorithm descriptions are accompanied by simulation results obtained for a specific network topology. In particular, the antenna system is simulated assuming a mobile network topology that is continuously changing. Basic results presented are the dependence of the overall network *throughput* on the design of the adaptive-antenna system, and on the properties of the adaptive-beamforming algorithms and associated antenna patterns.

Keywords: Smart antennas; land mobile radio cellular systems; land mobile radio data communications; mobile communication; adaptive arrays; land mobile radio equipment; array signal processing; spatial division multiple access; direction of arrival estimation; antenna array mutual coupling

1. Introduction

Part 2 of this paper provides descriptions of the signal-processing algorithms accompanying a smart-antenna system. Following the design of the planar antenna array, presented in Part 1, Part 2 continues by describing how signal-processing algorithms are used to detect and estimate the angles of arrival of the incoming signals, and presenting adaptive algorithms that can be used for beamforming. In particular, this paper describes how the functional components of a smart-antenna system interrelate (refer to Figure 1). After the smart-antenna system of Fig 1 is analyzed, its performance is examined in the presence of other smart-antenna systems in a wireless communication network with changing topology (see Figure 2). The wireless mobile network depicted in Figure 2 uses planar-array antennas as examples, and it has nodes that assume different roles, i.e., any node has the capability of relaying or routing information to neighboring nodes. Since there

is no server or base station in the network, links are created among nodes in an ad hoc manner.

With regard to the antenna system used in this network configuration, the nodes can use either omnidirectional antennas, or antennas with narrow and adaptive beams. When an omnidirectional antenna is used, all nodes within the range of the transmitting node must remain silent, to avoid collision, until transmission is completed. This situation is depicted in Figure 2a, where, for example, the communication devices are laptop computers, and they represent nodes in the network. On the other hand, if smart antennas are used as in Figure 2b, their narrow adaptive beams allow more nodes to communicate with each other simultaneously, without interfering with others, thereby increasing the network capacity.

The performance of a network is usually measured in terms of its overall *throughput*, which is the average number of information-bearing packets that successfully reach their destination during the time at which a single packet can be transmitted. Since some beamforming algorithms depend on the directions of arrival of all the incoming signals in order to design a beam pattern, the speed with which the direction-of-arrival estimator can accurately estimate the angles of arrival can also impact the throughput of this type of network. The ability of the beamformer to reject interference is affected by the size and geometry of the antenna array. Using a larger array allows the beamformer to design a pattern with a narrower main beam and a larger number of nulls. However, using a larger antenna array places a larger computational burden on the beamformer, which may even make the smart antenna too costly, or impractical to realize. Thus, it is observed that the designs of the beamformer, the direction-of-arrival estimator, and the antenna geometry impact the overall throughput of the wireless and mobile network depicted in Figure 2.

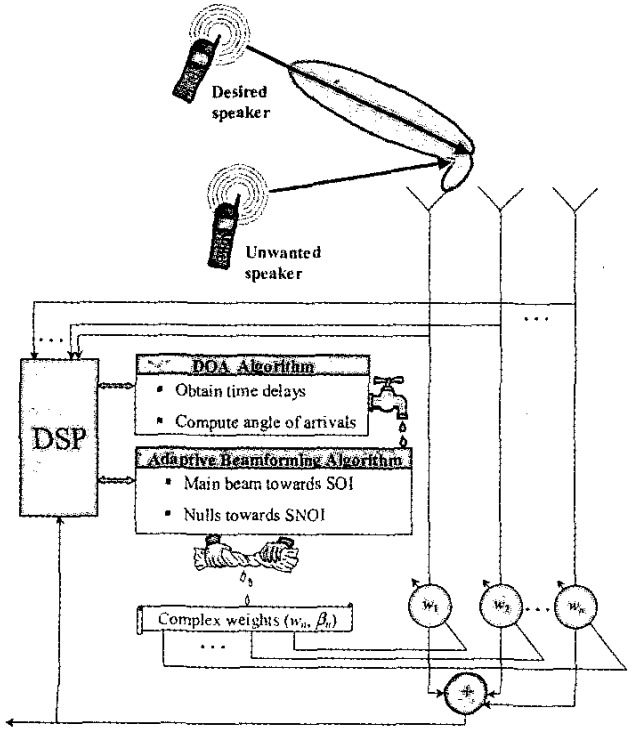

Figure 1. A functional block diagram of a smart-antenna system.

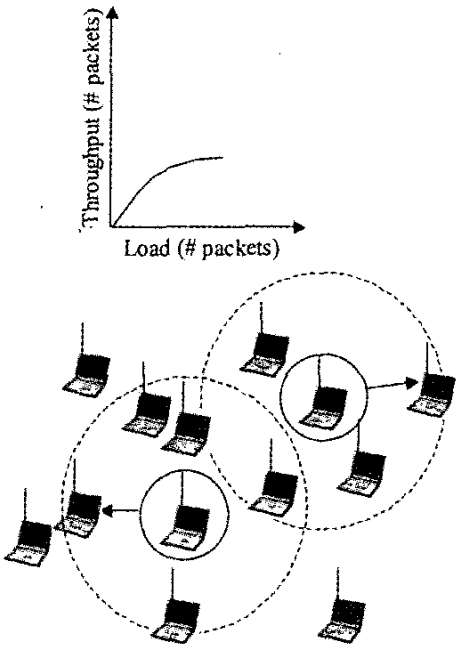

Figure 2a. A typical network using low-throughput omnidirectional connectivity.

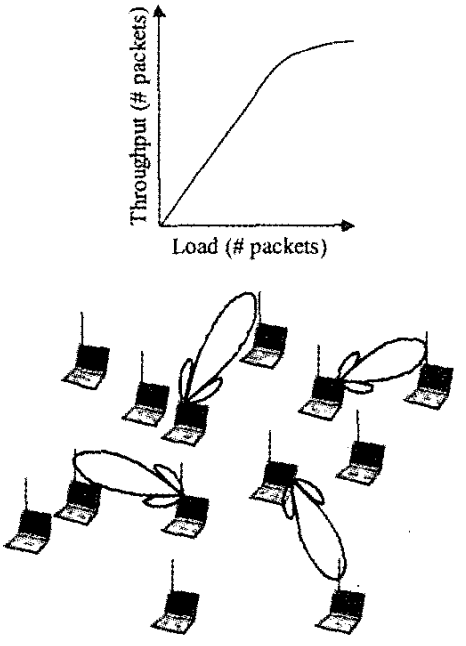

Figure 2b. A typical network using high-throughput adaptive directional connectivity.

2. Adaptive Signal-Processing Algorithms

Intelligence, based on the definition in Webster's dictionary, is the ability to gain/apply knowledge and to manipulate one's environment. Consequently, the amount of intelligence a system possesses depends on the information collected, how it gains knowledge from the processed information, and its ability to apply

this knowledge. In smart-antenna systems, this knowledge is gained and applied via algorithms processed by a digital signal processor (DSP), as shown in Figure 1. The objectives of a DSP are to estimate: 1) the direction-of-arrival (DOA) of all impinging signals from the time delays of each antenna element; and 2) the appropriate weights to scan the maximum radiation of the antenna pattern toward the signal of interest (SOI), and to place nulls toward the signal not of interest (SNOI). Hence, the work on smart antennas promotes research in adaptive signal-processing algorithms, such as DOA and adaptive beamforming. The DOA estimation involves a correlation analysis of the array signals, followed by eigenanalysis and signal/noise sub-space formation. In adaptive beamforming, the goal is to adapt the beam by adjusting the amplitude and phase of each antenna element such that a desirable pattern is formed.

This section presents a brief overview of classical and subspace-based DOA computation. Then, two types of adaptive beamforming methods are described: one that uses the DOA directly; and another that does not use the DOA information, but rather a temporal reference signal or training sequence. Finally, an adaptive beamformer that generates mutually compensated weights is described.

2.1 Direction of Arrival

As the signals are received from each antenna element, the DOA algorithm computes the angles of arrival of all impinging signals. There are many DOA algorithms found in the literature today, and some of them are described in [1]. The classical methods are based on the concept of measuring the power received from each direction. These algorithms determine the angles of arrival of the incoming signals by scanning the beam of the radiation pattern, and surveying the space for signals above a certain power threshold. These methods are known as low-resolution algorithms. They are unlike the more recently introduced high-resolution subspace-based algorithms, which make use of the underlying data model (described in detail, next) of the received data.

Consider an $M \times N$ planar array, with inter-element spacing d_x along the x axis, and d_y along the y axis, as shown in Figure 3. When an incoming wave, carrying a baseband signal $s(t)$, impinges at an angle (θ,φ) on the antenna array, it produces *time delays* relative to the signal received at the other antenna elements. These time delays depend on the antenna geometry, the number of elements, and the spacing between the elements. For the array of Figure 3, the time delay of the signal $s(t)$ at the (m,n)th element – relative to the reference element $(0,0)$, at the origin – is

$$\tau_{mn} = \frac{\Delta r}{v_0}, \tag{1}$$

where Δr and v_0 represent the differential distance and the speed of the light in free space, respectively. The differential distance, Δr, is computed using

$$\Delta r = d_{mn}\cos(\psi), \tag{2}$$

where d_{mn} is the distance between the origin and the (m,n)th element, and ψ is the angle between the radial unit vector from the origin to the (m,n)th element and the radial unit vector in the direction of the incoming signal, $s(t)$. Subsequently, d_{mn} and $\cos(\psi)$ are determined using

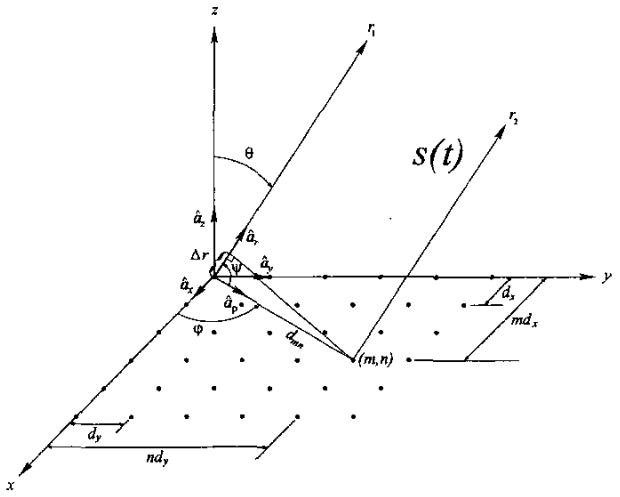

Figure 3. An $M \times N$ planar array, with a graphical representation of the time delay.

$$d_{mn} = \sqrt{m^2 d_x^2 + n^2 d_y^2},$$
$$\cos(\psi) = \frac{\hat{\mathbf{a}}_r \cdot \hat{\mathbf{a}}_\rho}{|\hat{\mathbf{a}}_r||\hat{\mathbf{a}}_\rho|}, \tag{3}$$

where $\hat{\mathbf{a}}_r$ and $\hat{\mathbf{a}}_\rho$ are the unit vectors along the direction of the incoming signal, $s(t)$, and along the distance, d_{mn}, to the (m,n)th element, respectively. Thus, the unit vectors (i.e., $\hat{\mathbf{a}}_r$ and $\hat{\mathbf{a}}_\rho$) are expressed as

$$\hat{\mathbf{a}}_r = \hat{\mathbf{a}}_x \sin\theta\cos\varphi + \hat{\mathbf{a}}_y \sin\theta\sin\varphi + \hat{\mathbf{a}}_z \cos\theta,$$
$$\hat{\mathbf{a}}_\rho = \frac{\hat{\mathbf{a}}_x m d_x + \hat{\mathbf{a}}_y n d_y}{\sqrt{m^2 d_x^2 + n^2 d_y^2}}, \tag{4}$$

where $\hat{\mathbf{a}}_x$, $\hat{\mathbf{a}}_y$, and $\hat{\mathbf{a}}_z$ are the unit vectors along the x, y, and z axes, respectively. Finally, substituting Equations (2)-(4) into Equation (1), the *time delay* of the (m,n)th element with respect to the element at the origin (i.e., $(0,0)$) is written as

$$\tau_{mn} = \frac{m d_x \sin\theta\cos\varphi + n d_y \sin\theta\sin\varphi}{v_0}. \tag{5}$$

Once the time delays are determined for each antenna element, they are part of the sampled signals received at the array. For example, the sampled signal received by the (m,n)th element at discrete time k contains the time delay τ_{mn}, and it is expressed as

$$x_k[m,n] = s(kT - \tau_{mn}) \tag{6}$$

for $m = 0,1,...,M-1$ and $n = 0,1,...,N-1$, where T is the sampling period. To keep the notation simple, the coordinates (m,n) are mapped into a sequence of integers from 0 to $MN-1$, using the mapping from $(m,n) \rightarrow i$ (i.e., $i = Nm+n$ for $m = 0,1,...,M-1$ and $n = 0,1,...,N-1$). Thus, Equation (6) can be rewritten as

$$x_k[i] = s(kT - \tau_i), \tag{7}$$

where the time delay, τ_{mn}, has been mapped to τ_i. For a digitally modulated baseband signal with symbol period T, the sampled baseband signal at time kT at the ith [i.e., $(m,n) \rightarrow i$] element is approximated by [1]

$$\begin{aligned} x_k[i] &\approx s(kT)e^{-j2\pi f \tau_i} + g_k[i] \\ &\approx s(kT)a_i(\theta,\varphi) + g_k[i], \end{aligned} \tag{8}$$

where f, $a_i(\theta,\varphi)$, and $g_k[i]$ represent the carrier frequency, an element of the *steering vector* of the signal $s(kT)$, and a sample of uncorrelated noise at the ith element, respectively. Now, if p baseband signals (i.e., $s_0(t), s_1(t), ..., s_{p-1}(t)$) impinge on the antenna array with different angles, (θ_q, φ_q), $q = 0,1,...,p-1$, the above equation is extended to

$$\begin{bmatrix} x_k[0] \\ x_k[1] \\ \vdots \\ x_k[MN-1] \end{bmatrix} = \begin{bmatrix} a_0(\theta_0,\varphi_0) & a_0(\theta_1,\varphi_1) & \cdots & a_0(\theta_{p-1},\varphi_{p-1}) \\ a_1(\theta_0,\varphi_0) & \ddots & & \vdots \\ \vdots & & & \\ a_{MN-1}(\theta_0,\varphi_0) & \cdots & & a_{MN-1}(\theta_{p-1},\varphi_{p-1}) \end{bmatrix} \begin{bmatrix} s_0(kT) \\ s_1(kT) \\ \vdots \\ s_{p-1}(kT) \end{bmatrix} + \begin{bmatrix} g_k[0] \\ g_k[1] \\ \vdots \\ g_k[MN-1] \end{bmatrix}. \tag{9}$$

In matrix notation, Equation (9) can be rewritten as

$$\mathbf{x}_k = \mathbf{A}\mathbf{s}_k + \mathbf{g}_k. \tag{10}$$

The columns of the matrix $\mathbf{A}$ represent the *steering vectors* of the impinging signals, and form a linearly independent set (assuming that each signal has a different angle of arrival). The set of all possible steering vectors is known as the *array manifold*, which includes the steering vectors corresponding to the incoming signals. For some array configurations, the array manifold is computed analytically, such as for uniform planar arrays (as an example), but for others, the manifold must be measured experimentally.

In order to use the steering vectors to compute the direction of arrival, it is necessary to examine the spatial-correlation matrix $\mathbf{R}_{xx}(k)$. This is defined as $\mathbf{R}_{xx}(k) = \mathcal{E}\left[\mathbf{x}_k \mathbf{x}_k^H\right]$, where $\mathcal{E}[\bullet]$ is the expectation operator. The elements of $\mathbf{R}_{xx}(k)$ describe how the signals received by the antenna elements are correlated. In general, $\mathbf{R}_{xx}(k)$ is not known a priori, and it needs to be estimated using an exponentially weighted estimate. The estimate of $\mathbf{R}_{xx}(k)$ is written as

$$\mathbf{R}_{xx}(k) = \alpha \mathbf{R}_{xx}(k-1) + (1-\alpha)\mathbf{x}_k \mathbf{x}_k^H, \tag{11}$$

where α is referred to as the *forgetting factor*, with $0 < \alpha < 1$. If p signals impinge upon the array, then $\mathbf{R}_{xx}(k)$ contains p large eigenvalues compared to the rest of the $MN-p$ eigenvalues. The p eigenvectors corresponding to those p eigenvalues span what is called the *signal subspace*, and the space spanned by the eigenvectors corresponding to the remaining $MN-p$ eigenvalues is called the *noise subspace*. Moreover, these two subspaces are orthogonal to each other. Since the steering vectors corresponding to the p signals span the same subspace as the eigenvectors corresponding to the largest p eigenvalues, they are also orthogonal to the noise subspace [2]. Thus, the directions of arrival are determined by searching through the array manifold corresponding to all angles, and finding the p elements that are most orthogonal to the estimated noise subspace. The algorithm that uses this strategy is referred to as the *MUltiple SIgnal Classification* (MUSIC) algorithm [3]. The advantage of this algorithm is that it exhibits high

Table 1. The signals used to test the smart-antenna system of this paper.

	SOI		SNOI	
	θ_0	φ_0	θ_0	φ_0
Case 1	0°	0°	45°	0°
Case 2	30°	45°	60°	45°

SOI: Signal of interest; SNOI: Signal not of interest

Table 2. ESPRIT simulation results for the two cases of Table 1, based on 500 samples.

Description		SOI		SNOI	
		θ_0	φ_0	θ_0	φ_0
Case 1	Without noise	0.000°		45.000°	0.000°
Case 2	Without noise	30.000°	45.000°	60.000°	45.000°
Case 1	AWGN – mean = 0, var. = 0.1	0.030°		44.945°	0.000°
Case 2	AWGN – mean = 0, var. = 0.1	30.004°	44.955°	60.060°	44.973°
Case 1	Mutual coupling	0.0508°		44.509°	0.0133°
Case 2	Mutual coupling	30.138°	45.719°	61.072°	45.460°

resolution. However, it can be computationally intensive, since it requires a search through the entire array manifold for the steering vectors that are orthogonal to the noise subspace.

Several other subspace-based DOA estimators are available. One class of these algorithms is known as the *Estimation of Signal Parameters via Rotational Invariance Techniques* (ESPRIT) [2]. This class of algorithms also provides the high resolution of MUSIC, but it does not require a costly search. The ESPRIT algorithm allows the DOAs to be computed directly, and has been used with different array geometries, including planar arrays [4-6].

The unitary ESPRIT [5] algorithm has been implemented to illustrate its use in computing both θ and φ with the designed planar array of Part 1 of this paper. Using the signals listed in Table 1 as input signals to the unitary ESPRIT, it was observed to give accurate results in the presence of noise and mutual coupling (see Table 2).

2.2 Adaptive Beamforming

An adaptive beamformer consists of 1) multiple antennas; 2) complex weights, the function of which is to amplify/attenuate and delay the signals from each antenna element; and 3) a summer to add all of the processed signals, in order to tune out the signals not of interest, while enhancing the signal of interest. Hence, beamforming is sometimes referred to as *spatial filtering*, since some incoming signals from certain spatial directions are filtered out, while others are amplified. In short, spatial filtering is analogous to designing a finite impulse response (FIR) filter for filtering a time-domain signal.

For the planar array of Figure 3, the samples of the received signal vector, $\mathbf{x}_k$, in Equation (10) are multiplied by a complex weight, w, the magnitude of which represents the gain/attenuation, and the phase of which represents a delay or shift. The weighted elements are then summed to form the beamformer output, y_k. This can be expressed as the inner product of $\mathbf{x}_k$ and $\mathbf{w}$ (a vector of size $MN \times 1$, the elements of which are the complex weights). Thus, the response of the beamformer to a signal from direction (θ,φ), in the absence of noise, is computed as

$$\begin{bmatrix} x_k[0] \\ x_k[1] \\ \vdots \\ x_k[MN-1] \end{bmatrix} = \begin{bmatrix} a_0(\theta,\varphi) \\ a_1(\theta,\varphi) \\ \vdots \\ a_{MN-1}(\theta,\varphi) \end{bmatrix} s(kT),$$

$$y_k = \mathbf{w}^H \mathbf{x}_k = \mathbf{w}^H \mathbf{a}(\theta,\varphi) s(kT). \tag{12}$$

The weights in Equation (12) are obtained using an adaptive-beamforming algorithm. Adaptive-beamforming algorithms are classified as either DOA-based, temporal-reference-based, or signal-structure-based [7]. In DOA-based beamforming, the direction-of-arrival algorithm passes the DOA information to the beamformer, as illustrated in Figure 1. This is used to design a radiation pattern with the main beam directed toward the signal of interest, and with nulls in the directions of the interferers. One example of a DOA-based beamformer is the Minimum Variance Distortionless Response (MVDR) [8] beamformer. Given the DOA information of the signal of interest, the MVDR beamformer designs the beamformer weights by minimizing the output power of the beamformer, subject to the constraint that the response of the beamformer should be unity in the direction of the signal of interest [i.e., $\mathbf{w}^H \mathbf{a}(\theta,\varphi) = 1$]. This minimization produces a beamformer with nulls in the directions of the interfering signals, and a maximum directed toward the desired signal. The MVDR beamformer computes the weights of each antenna element as

$$\mathbf{w}_{MVDR} = \frac{\mathbf{R}_{xx}^{-1}(n)\mathbf{a}(\theta,\varphi)}{\mathbf{a}^H(\theta,\varphi)\mathbf{R}_{xx}^{-1}(n)\mathbf{a}(\theta,\varphi)}, \tag{13}$$

where (θ,φ) and $\mathbf{R}_{xx}^{-1}(n)$ are the angle of arrival of the signal of interest provided by the DOA; and the inverse of the correlation matrix, $\mathbf{R}_{xx}(n)$ (which is estimated as in Equation (11)], respectively.

On the other hand, temporal-reference beamformers use a known training sequence to adjust the weights, and to form a radiation pattern with a maximum towards the signal of interest and nulls towards the signals not of interest. Specifically, if $d(k)$ denotes the sequence of reference or training symbols known a priori at the receiver at time k, an error, $\varepsilon(k)$, is formed as the difference between the beamformer output, $\mathbf{w}^H \mathbf{a}(\theta,\varphi)$, and $d(k)$ (i.e., $\varepsilon(k) = d(k) - \mathbf{w}^H \mathbf{a}(\theta,\varphi)$). This error signal is used by the beamformer to adaptively adjust the complex weights, $\mathbf{w}$, so that the mean-squared error (MSE) is minimized. The choice of weights that minimize the MSE is such that the radiation pattern has a beam in the direction of the source that is transmitting the reference signal, and that there are nulls in the radiation pattern in the directions of the interferers. Once the beamformer has locked onto the reference signal, then the complex weights are maintained as fixed, and transmission of the data packet begins.

One temporal-reference beamformer that minimizes the MSE is the least-mean-square (LMS). The complex LMS algorithm computes the complex weights $\mathbf{w}_k$ iteratively, using [9]

$$\mathbf{w}_{k+1} = \mathbf{w}_k - 2\mu \mathbf{x}_k \varepsilon(k), \tag{14}$$

where μ denotes the step size, which is related to the rate of convergence: in other words, how fast the LMS algorithm reaches steady state. The smaller the step size, the longer it takes the LMS algorithm to converge. This means that a longer reference or training sequence is needed, which would reduce the payload and, hence, the bandwidth available for transmitting data. Throughput issues will be discussed later, in Section 3.

The complex weights, $\mathbf{w}_k$, computed by Equation (14) are the ideal weights in the absence of mutual coupling. When these complex weights are used in the presence of mutual coupling, degraded far-field patterns are obtained, unless a compensation is made to the weights to account for coupling. In [10], these effects were modeled as a multiplication process of the inverse mutual-coupling matrix (i.e., $\mathbf{C}^{-1}$) in Equation (3) of Part 1 and the input signals, $\mathbf{x}_k$. Thus, in order for the LMS to generate compensated weights that ideally cancel these effects, the inverse process needs to be applied; that is, the input signals, $\mathbf{x}_k$ in Equation (14), must be multiplied by $\mathbf{C}$ [11].

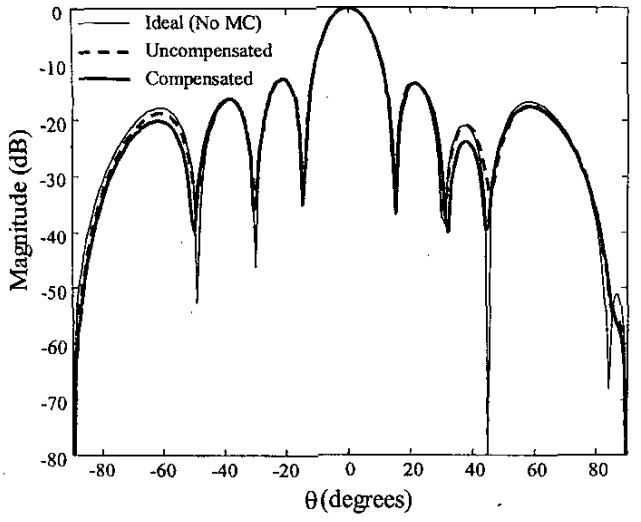

Figure 4a. The E-plane ($\varphi = 0°$) amplitude pattern for Case 1 of Table 1 (the microstrip planar array of Figure 1 in Part 1).

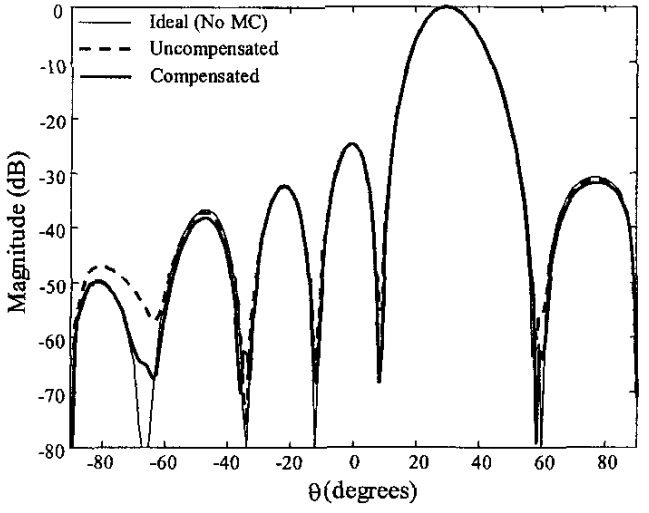

Figure 4b. The amplitude pattern for Case 2 of Table 1 along the $\varphi = 45°$ plane, for the microstrip planar array of Figure 1 in Part 1.

To illustrate how the adaptive beamformer shapes the radiation pattern from the information supplied by the DOA algorithm, and how compensation for mutual coupling improves the SINR [signal-plus-interference-to-noise ratio], the results of the ESPRIT algorithm, listed in Table 2, were used. For the first case listed in Table 1, the resulting E-plane patterns are shown in Figure 4a. The first pattern (the solid thin line) illustrates how well the LMS algorithm rejected the interferer at $\theta_0 = 45°$, $\varphi_0 = 0°$, while placing the maximum of the radiation pattern toward the signal of interest at $\theta_0 = 0°$, in the absence of mutual coupling. The second pattern (dashed line), generated using the ideal (uncompensated) excitations of the LMS in *Ensemble*® [12], shows the undesired effects of mutual coupling, such as a shallow and shifted null at the location of the signal not of interest. On the other hand, when compensation was made in these excitations for mutual coupling, *Ensemble*® [12] showed an improvement of 6.3 dB at the location of the signal not of interest (see the solid thick line in Figure 4a). The second case listed in Table 1, the $\varphi = 45°$ radiation patterns of Figure 4b, show similar results. Here, a higher improvement of 8.1 dB was observed at the location of the signal not of interest for the compensated pattern (the solid thick line) over the uncompensated pattern (the dashed line). Therefore, weights that take mutual coupling into account gave superior system performance.

3. Smart Antenna Systems for Wireless and Mobile Networks

In wireless and mobile networks, the use of directional beams for communication results in reduced interference and, hence, improved capacity. The following section presents some simulation results that show how the capacity of a wireless network depends on the size of the antenna array, the beam pattern used, and the speed with which the beamformer/direction-of-arrival estimator can compute an appropriate beam pattern.

3.1 The Protocol

The protocol described in this section is based on the IEEE 802.11 Medium Access Control (MAC) [13] for Time Division Multiple Access (TDMA) environment, the details of which can be found in [14]. The channel-access protocol exploits the fact that the interference from a node using directional antennas is low, and allows its neighbors to access the channel if the sensed signal power is below a certain threshold. It also allows nodes to exchange training signals before the data or packet transfer, for beamforming purposes. Each node starts with an isotropic mode so that it can receive signals from everywhere in space. Then, once a signal is detected, the node switches to directional mode by forming a beam toward the transmitting node. Packet transfer takes place in the directional mode, once the beams have been formed. It should be emphasized that the introduction of training packets incurs an overhead in the data traffic. If the beamforming algorithms are slow to adapt themselves, the required training-packet length will have to be longer, leading to lower network capacity.

3.2 Simulations

The main objective of the simulations is to qualitatively analyze the capacity improvement in wireless networks when smart antennas are used for communication. The simulations also exam-

Table 3. Packet lengths and time intervals used in the protocol simulations.

	Control Signals				Beamforming		Control Signal	Payload
Packet Type/Interval	DIFS	SIFS	RTS	CTS	TXTRN	RXTRN	ACK	DATA
Length	0.014L	0.003L	0.007L	0.007L	Variable	Variable	0.007L	L

ine the dependence of capacity on various antenna patterns, and on the length of the training packets.

An ad hoc network of 55 nodes was chosen and simulated using the *OPNET*® [15] Modeler/Radio tool. The load at each node was assumed to be Poisson-distributed. Table 3 shows the values used in the simulations for various packet lengths and time intervals specified in the protocol. All packet lengths were normalized to the payload or DATA packet length. The lengths of the reference signals (TXTRN and RXTRN) were made variable, to analyze the performance of the protocol for different lengths.

The network capacity for various antenna patterns was evaluated, in order to guide the antenna design for high network capacity. The training-packet length was chosen to be 10% of the payload (DATA) length. The average network *throughput* was measured, for planar arrays of size 8×8 and 4×4, with Tschebyscheff (–26 dB sidelobe level) and uniform excitation distributions. For this simulation, while the maxima of all patterns were toward the signal of interest, neither of the two Tschebyscheff patterns nor the one with uniform excitation had been adapted to place the nulls toward the signals not of interest. Figure 5 shows the average network throughput (the average number of successfully transmitted packets in the network during a packet time) as a function of the average load (the average number of packets generated in the network during a packet time), for various antenna patterns. In addition, the figure shows that the network throughput for the 8×8 array size was greater, when compared to the throughput for the 4×4 array size. This can be attributed to the smaller beamwidth of the 8×8 array, which leads to lower co-channel interference.

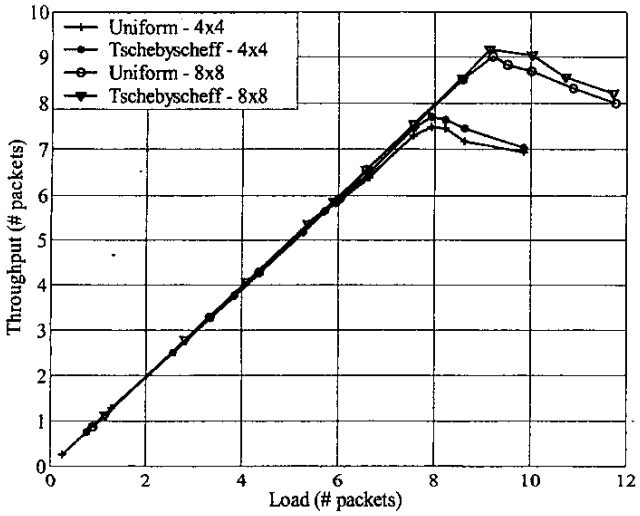

Figure 5. Curves showing the throughput as a function of load for different antenna patterns.

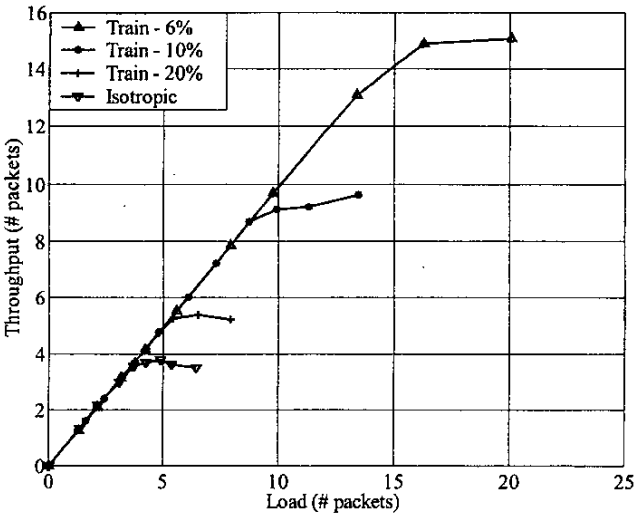

Figure 6. Curves showing the throughput as a function of load for different training periods.

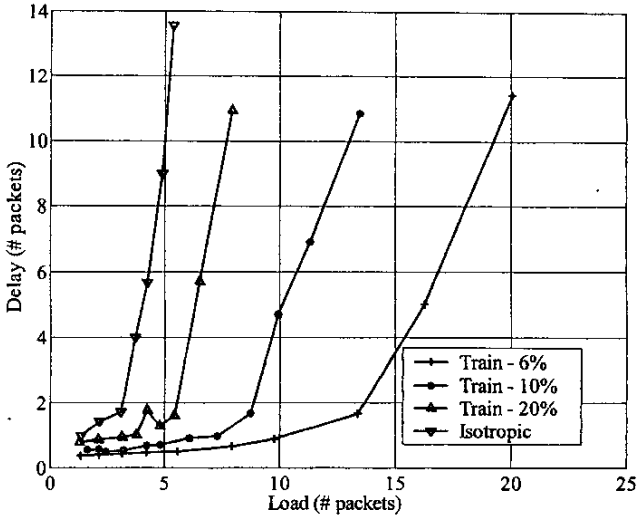

Figure 7. Curves showing the delay as a function of load for different training periods.

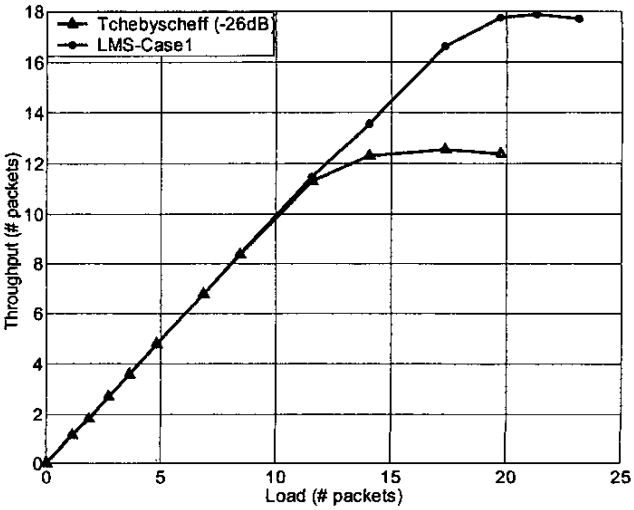

Figure 8. A comparison between the throughput for a fixed Tschebyscheff pattern with a –26 dB sidelobe level and the pattern for Case 1 of Table 1.

The network capacity for various training-packet lengths was evaluated, in order to guide the design of beamforming algorithms for high network capacity. The nodes were assumed to be equipped with 8×8 planar arrays of microstrip-patch antennas, with non-adapted Tschebyscheff (–26 dB sidelobe level) excitation distributions. In other words, the shape of the beam pattern was fixed to be

Tschebyscheff, and was simply reoriented in the direction determined by the direction-of-arrival estimator. Figure 6 shows the average network throughput as a function of the average load for the cases when the training packet-length was 6%, 10%, and 20% of the payload. An 8×8 planar array with a non-adapted Tschebyscheff pattern (–26 dB sidelobe level) was used. Figure 7 shows the average packet delay (the average delay experienced by a packet before it was received by the destination) as a function of the average load for the same training-packet lengths and the same array. As can be seen from these figures, the network throughput dropped and the packet delays increased rapidly with increasing training-packet size. Also, Figure 6 shows that the throughput of the network was higher when smart/directional antennas were used instead of isotropic antennas.

The network throughput was further analyzed using the LMS-algorithm-generated adapted pattern, shown in Figure 4a. This was formed to have the maximum toward the signal of interest, and to have the null toward the signals not of interest. In Figure 8, the throughput for this case is compared to the throughput of a fixed Tschebyscheff non-adapted antenna pattern (–26 dB sidelobe level) that did not have a null toward the signals not of interest. From the results in this figure, it can be concluded that the adaptive LMS-beamforming-algorithm pattern leads to higher throughput. This is attributed to the fact that the LMS-generated adapted pattern had a null toward the signals not of interest, while the Tschebyscheff pattern did not posses such an attribute, even though the Tschebyscheff pattern exhibited much lower minor lobes than the LMS-generated pattern [16].

4. Conclusions

Certain guidelines for designing smart-antenna systems for optimum capacity in wireless and mobile networks have been discussed. Antenna parameters, such as array size and excitation distribution, can be chosen to meet the capacity requirements for a network. In fact, based on the simulation results, antennas with narrower pattern beamwidth (i.e., larger arrays) lead to provide higher *throughput*, as would be expected. However, there is a trade-off: larger arrays require more training bits and, hence, the overall throughput is affected, as well. Also, antennas that exhibit adaptive patterns with maxima toward the signal of interest and nulls toward the signal not of interest usually lead to higher throughput, compared to non-adaptive patterns (that do not have the nulls toward the signals not of interest), even if the non-adaptive patterns may have lower minor lobes.

Furthermore, network capacity was evaluated, in order to guide the design of beamforming algorithms for high network capacity. Since there is a trade-off between the network capacity and the training-packet length, these simulations can assist in choosing a suitable value for the training-packet length, without compromising the network capacity. The training period places an upper bound on the convergence speed of the beamforming and DOA-estimation algorithms, serving as a guideline for the algorithm design. The results showed that training periods greater than 20% considerably reduce the throughput. Therefore, it can be inferred that fast beamforming algorithms are critical for high network capacity.

Employment of smart-antenna systems in wireless and mobile networks creates a wide scope for enhancing the network capacity. Through the design of efficient channel-access protocols, the spatial diversity of smart antennas can be exploited to increase the capacity of a wireless network. However, the design of such protocols requires a careful consideration of the system aspects of the smart-antenna technology. In this work, a channel-access protocol was suggested for wireless and mobile networks employing smart antennas to communicate (for details, refer to [14]). This protocol was built based on the Medium Access Control (MAC) protocol of the IEEE 802.11 Wireless Local Area Network (LAN) Standard [13] for Time Division Multiple Access (TDMA) environment. The protocol facilitates the use of smart antennas and decreases co-channel interference, thereby increasing the capacity of the network. In addition, by accounting for the effects of mutual coupling, it produces radiation patterns with deeper nulls at the locations of the signals not of interest, thus further increasing the network throughput.

5. Acknowledgements

The authors would like to thank Ravi Govindarajula and Dr. Jeffrey M. Capone for generating and providing the data in Figures 5-8.

6. References

1. L. C. Godara, "Application of Antenna Arrays to Mobile Communications, Part II: Beam-Forming and Direction of Arrival Considerations," *Proceedings of the IEEE*, **85**, 8, August 1997, pp. 1195-1254.

2. R. H. Roy and T. Kailath, "ESPRIT – Estimation of Signal Parameters via Rotational Invariance Techniques," *IEEE Transactions on Acoustics, Speech, and Signal Processing*, **ASSP-37**, July 1989, pp. 984-995.

3. P. Strobach, "Bi-Iteration Multiple Invariance Subspace Tracking and Adaptive ESPRIT," *IEEE Transactions on Signal Processing*, **48**, 2, February 2000, pp. 442-456.

4. P. Strobach, "Two-Dimensional Equirotational Stack Subspace Fitting with an Application to Uniform Rectangular Arrays and ESPRIT," *IEEE Transactions on Signal Processing*, **48**, July 2000, pp. 1902-1914.

5. M. D. Zoltowski, M. Haardt, and C. P. Mathews, "Closed-Form 2-D Angle Estimation with Rectangular Arrays in Element Space or Beamspace via Unitary ESPRIT," *IEEE Transactions on Signal Processing*, **44**, February 1996, pp. 316-328.

6. A. L. Swindlehurst, B. Ottersten, R. Roy, and T. Kailath, "Multiple Invariance ESPRIT," *IEEE Transactions on Signal Processing*, **40**, April 1992, pp. 867-881.

7. A. O. Boukalov and S. G. Haggman, "System Aspects of Smart-Antenna Technology in Cellular Wireless Communications – An Overview," *IEEE Transactions on Microwave Theory and Techniques*, **MTT-48**, June 2000, pp. 919-929.

8. J. Capon, "High Resolution Frequency-Wavenumber Spectral Analysis," *Proceedings of the IEEE*, **57**, August 1969, pp. 1408-1518.

9. B. Widrow and S. D. Stearns, *Adaptive Signal Processing*, Englewood Cliffs, NJ, Prentice Hall, 1985.

10. I. J. Gupta and A. A. Ksienski, "Effect of Mutual Coupling on the Performance of Adaptive Arrays," *IEEE Transactions on Antennas and Propagation*, **AP-31**, 5, September 1983.

11. H. Steyskal and J. S. Herd, "Mutual Coupling Compensation in Small Array Antennas," *IEEE Transactions on Antennas and Propagation*, **AP-38**, 12, December 1990, pp 1971-1975.

12. Ansoft Corp., *Ensemble*®: http://www.ansoft.com/products/hf/ensemble/.

13. IEEE Standards Dept. (P802.11), *IEEE Standard for Wireless LAN Medium Access Control (MAC) and Physical Layer (PHY) Specifications*, IEEE Std 802.11, November 1997.

14. R. Govindarajula, "Multiple Access Techniques for Mobile Ad Hoc Networks," MS Thesis, Arizona State University, May 2001.

15. OPNET Technologies, Inc.™, *OPTNET*®: http://www.opnet.com.

16. S. Bellofiore, J. Foutz, R. Govindarajula, I. Bahceci, C. A. Balanis, A. S. Spanias, J. M. Capone and T. M. Duman, "Smart Antenna System Analysis, Integration and Performance for Mobile Ad-Hoc Networks (MANETS)," *IEEE Transactions on Antennas and Propagation*, **AP-50**, 5, May 2002, pp. 571-581.